

# Electronic structure modelling of edge-functionalisation of graphene by $\text{Mn}_x\text{O}_y$ particles — Electronic Supporting Information

Richard N.L. Terrett<sup>\*1</sup>, George Tsekouras<sup>2</sup>, Takuya Tsuzuki<sup>2</sup>,  
Gerhard F. Swiegers<sup>3</sup>, Ronald J. Pace<sup>1</sup>, and Robert Stranger<sup>1</sup>

<sup>1</sup>Computational Quantum Chemistry Group, Research School of Chemistry, Australian  
National University, Canberra, Australian Capital Territory, 0200, Australia

<sup>2</sup>Research School of Electrical, Energy and Materials Engineering, Australian National  
University, Canberra, Australian Capital Territory, 0200, Australia

<sup>3</sup>Intelligent Polymer Research Institute, Australian Institute for Innovative Materials,  
University of Wollongong, Wollongong, New South Wales, 2522, Australia

15 November 2020

## 1 Commentary on IBSI analysis of Mn-terminal lig- and and hydrogen-bonding interactions in cluster models

Further analysis of the terminal ligand environments and hydrogen bonding networks of **ch**-wide and **ch**-tall was performed using the IBSI metric, computed using the MultiWfn software with a radial cutoff of 350 pm and an integration quality of ‘ultrafine’. Results for Mn–OH<sub>2</sub>, Mn–OH, and hydrogen bonding interactions are given in Table 1. These data indicate that the strength of Mn–OH<sub>2</sub> bonds within this cluster are competitive with the strength of hydrogen bonding interactions between ligands, supporting the interpretation that modulation of hydrogen bonding interactions by the dielectric environment of the molecule is responsible for reorientation of terminal ligands, and that these reorientations are low-energy phenomena. Klein, *et al.* [1] consider the diagnostic IBSI range for transition metal coordination 0.15–0.60,<sup>a</sup> which suggests that *aqua* ligands in **ch**-wide and **ch**-tall are exceptionally labile.

<sup>a</sup>Note, however that their benchmark dataset does not include Mn–O bonds.

**Table 1:** IBSI values for covalent and noncovalent interactions in **ch**-wide and **ch**-tall.

Species	IBSI		
	Mn–OH <sub>2</sub>	Mn–OH	H–bonds
<b>ch</b> -tall, gas phase	0.06±0.00	0.16±0.01	—
<b>ch</b> -tall, solvated	0.07±0.00	0.16±0.00	0.03±0.00
<b>ch</b> -wide, gas phase	0.07±0.00	0.14±0.00	0.05±0.00
<b>ch</b> -wide, solvated	0.08±0.00	0.15±0.00	—

## 2 Determination of graphene-consistent inter-pin distance

The procedure adopted for determining the distance between successive graphene zig-zag edge attachment points proceeds from the optimisation of a  $6 \times 7$  rectangular graphene sheet at a BP86/6-31G\* level of theory. The salient carbon atoms of the graphene edge are approximately  $246 \pm 0$  pm apart, whilst the second rank of carbon atoms are  $246 \pm 1$  pm apart. The small but nonzero variance in these data is due to the finite size of the graphene sheet considered, which results in slight distortions at the corners of the sheet with respect to the centers of the edges. Under periodic boundary conditions, a constant inter-carbon separation is anticipated. The quasi-periodic nature of the graphene edge structure is fortuitous, as it implies that simulations of arbitrary graphene attachment configurations are accessible by mere linear transit of the pins in approximately 246 pm increments.

## 3 Rationale for graphene-consistent ligand constraint model

A number of potential routes were identified for the simulation of oxo-manganese clusters attached to graphene sheets by edge functionalisation. These include **a**) the complete simulation of the graphene/oxo-manganese complex chelate by DFT, **b**) the use of a hybrid quantum-mechanical/molecular-mechanical (QM/MM) model which partitions the molecule into a relatively small region of interest which is described at a QM level of theory, and the remainder of the molecule, which is described using molecular mechanics, **c**) a QM/QM approach similar to the previously described QM/MM approach, where the majority of the graphene nanosheet is described using a computationally inexpensive QM approximation such as AM1, PM3 or density functional tight binding (DFTB), or DFT with a lower-quality basis set, and **d**) the simulation of cluster attachment to the graphene nanosheet *via* ‘graphene-consistent ligand constraints’, whereby the conformational influence of graphene attachment is modelled by geometric constraints applied to the terminal atoms of the EFG ligands.

We identified two simulation strategies as realisable within the constraints of available computational resources. These are the simulation of an isolated cluster using implicit graphene-consistent ligand constraints, and simulation of an explicit graphene/cluster chelate complex using heterogeneous basis sets.

**Table 2:** Quadratic fits in three variables ( $E = v_0(x + v_1)^2 + v_2$ ) for linear transits of graphene-consistent ligand constraints for three oxo-manganese clusters

Model	$v_0$ (/kJ · mol <sup>-1</sup> · nm <sup>-2</sup> )	$v_1$ (/nm)	$v_2$ (/kJ · mol <sup>-1</sup> )	$R^2$
<b>Homogeneous basis</b>				
<b>ch-wide</b>	251.65	-1.28	18.18	0.986
<b>ch-tall</b>	261.36	-1.11	2.93	0.966
<b>cu</b>	104.09	-1.22	7.24	0.845
<b>Heterogeneous basis</b>				
<b>ch-wide</b>	220.39	-1.29	19.45	0.986
<b>ch-wide</b>	267.94	-1.11	2.69	0.965
<b>cu</b>	91.75	-1.25	7.20	0.896

Simulation of an explicit chelate complex using homogeneous high quality basis functions was found to be infeasible due to computational expense and extreme difficulty in obtaining self-consistent field (SCF) convergence. QM/MM and mixed-Hamiltonian QM/QM approaches are also excluded due to a lack of required capabilities in ORCA at present.

## 4 Quadratic fits for linear transits of graphene-consistent ligand constraints

Quadratic fits for potential energy surfaces associated with linear transit of graphene-consistent ligand constraints for **ch-wide**, **ch-tall**, and **cu** are given in Table 2.

These data were compared with analogous calculations which employed a heterogeneous basis set (def2-TZVP on oxo-manganese core and coordinating carboxylate carbon and oxygen atoms, 6-31G\* elsewhere). In all cases near-indistinguishable results to the higher-quality calculations were obtained. These calculations were undertaken to confirm the suitability of heterogeneous basis sets for integrated graphene/cluster models.

## 5 Dual dihedral transit of amidobenzoic acid ligand attached to graphene nanosheet

Here we expand upon attempts to create a tractable model of the steric contribution to cluster coordination. We explored the viability of creating a two-parameter model for the conformational energy of an amidobenzoic acid ligand attached to a graphene zig-zag edge. This exploration was motivated by the possibility that **a**) it would explain the steric component of the conformational energy of cluster attachment as a function of a pair of dihedral angles ( $\phi_1$  and  $\phi_2$ , indicated in Figure 1), and that **b**) these dihedral angles could be predicted from graphene-consistent ligand constraint (GCLC) geometries, based on the assumption that the graphene edge does not severely deviate from planarity. To this end, a model was constructed consisting of a *p*-amidobenzoic acid moiety connected to the zig-zag edge of a graphene nanosheet, depicted in full

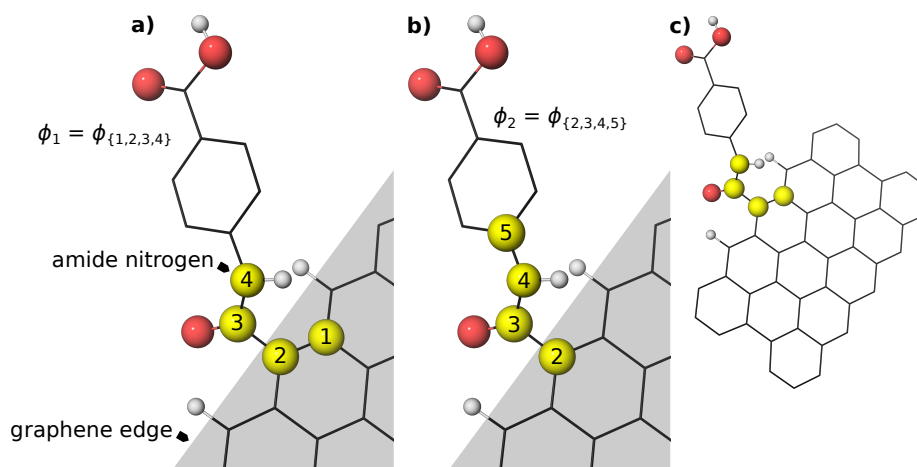


**Figure 1:** Dihedral angles  $\phi_1$  and  $\phi_2$  of *p*-amidobenzoic acid ligand. Note steric clash between amide nitrogen proton and graphene edge proton. **a)** Atoms constituting  $\phi_1$  indicated with yellow balls on cropped region, **b)** Atoms constituting  $\phi_2$  indicated with yellow balls on cropped region, **c)** Complete model geometry. Non-polar protons not relevant to steric interactions have been hidden for clarity.

in Figure 1c.  $\phi_1$  was transitioned from 40 to 60° in 5° increments, whilst  $\phi_2$  was transitioned from 130 to 180° in 10° increments. The calculation was performed at a 6-31G\* level of theory.

The relative energy at each transit point is depicted in Figure 2. It was found that the conformational energy was essentially insensitive to  $\phi_1$  over the inspected domain, a result which is consistent with ligand dihedral angle results previously presented (Main Text, Figure 11). Despite large differences in interligand distances in the **ch**-wide series indicated (0.479 nm), the  $\phi_1$  value is constrained within a narrow range of 50.1 to 56.1°. This range coincides with the potential energy basin of the transit of this variable (Main Text, Figure 11). On the other hand, the value of  $\phi_2$  spans 25.9°, with a corresponding energy range of approximately 8 kJ · mol<sup>-1</sup> per ligand. Transit of the  $\phi_2$  variable principally varies the degree of sp<sup>2</sup>/sp<sup>3</sup> character of the amide nitrogen. At ( $\phi_1, \phi_2$ ) coordinates consistent with a bound **ch**-wide cluster at a 4 ring separation, the expected steric contribution of this model is approximately 10 kJ · mol<sup>-1</sup>. This energy falls short of the 19.7 kJ · mol<sup>-1</sup> steric contribution recovered by the energetic decomposition analysis performed on **ch**-wide (Main Text, Section 3.8), although not alarmingly so. Moreover, as previously detailed, (Main Text, Section 3.8) comparison between the isodesmic series of graphene-integrated **ch**-wide clusters and GCLC models strongly suggests that the overall steric contribution to the conformational energy of cluster attachment is a quasi-constant quantity. Therefore, the range of conformational energies implied for differing interligand separations in the present two-parameter model suggests that it incompletely describes the steric contribution.

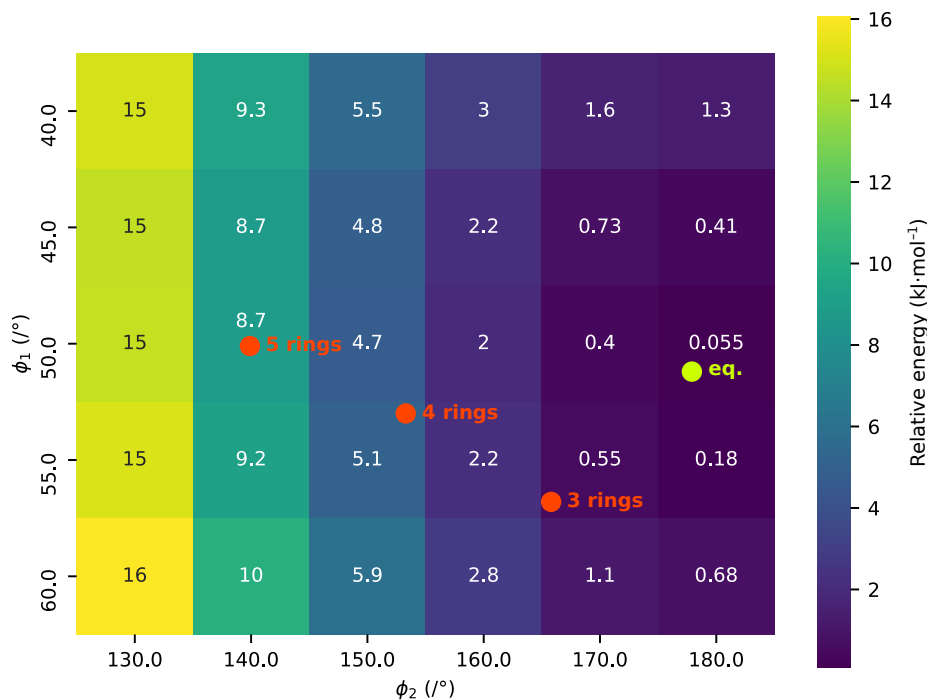


**Figure 2:** ‘Heatmap’ plot of relative energy of *p*-amidobenzoic acid ligand with dihedral angles  $\phi_1$  and  $\phi_2$ . *n.b.* markers indicating  $(\phi_1, \phi_2)$  coordinates of unconstrained model ( $E_{rel.} = 0.0 \text{ kJ}\cdot\text{mol}^{-1}$ ) and  $(\phi_1, \phi_2)$  coordinates of integrated **ch**-wide models at 3–5 rings of separation.

## 6 Technical information on cluster coordination energy decomposition

As indicated in the main text (Section 3.8), the conformational energy associated with cluster attachment may be decomposed into several components. Here, we expand upon the steric deformations to the amidobenzoate ligands incurred by graphene coordination, as well as the details of the energetic decomposition.

In a generic sense, the steric component of the energy of graphene-bound clusters was obtained by extracting a subset of the graphene-integrated geometry analogous to a GCLC model, and terminated by PMPAB or MMPAB ligands. We denote this a ‘clip-out’ model. The terminal propenyl moiety is obtained from the corresponding carbons of the graphene nanosheet. These carbons are protonated and a constrained optimisation is performed on *only these protons* to obtain  $E_1$ . Subsequent to this optimisation, a second optimisation is performed, where all nuclear positions are allowed to optimise except for the three terminal propenyl carbons, obtaining energy  $E_2$ . The energy  $E_{steric}^{clus.} = E_2 - E_1$ : this relaxation approximates the energy associated with steric collision between the graphene nanosheet edge and the chelating ligands. Note that the terminal propenyl moieties of the ligands are intentionally constrained in a non-equilibrium configuration (because the carbon–carbon distances of the graphene edge are approximately equivalent, whereas the single and double

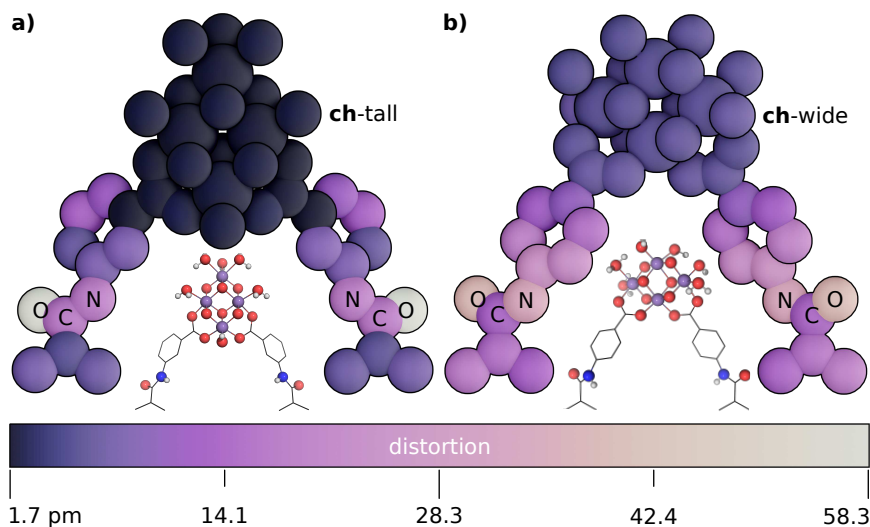


**Figure 3:** Absolute Cartesian displacement of atomic coordinates upon relaxation of steric deformation of **ch-tall** and **ch-wide** models clipped from graphene-integrated models.

bond of a propenyl moiety break that symmetry), however this constraint is maintained at each optimisation step and therefore does not contribute to the relative energy of any state.

The second conformational energy component,  $E_{pin}^{clus.}$ , is obtained by calculating the energy  $E_{pin}^{clus.} = E_3 - E_2$ , where  $E_3$  is obtained by the relaxation of all atomic positions in the ‘clip-out’ model, with the exception of the three interatomic distances between the propenyl carbon atoms of each ligand. This constraint ensures that the propenyl moieties maintain internal geometries consistent with the graphene edge carbons from which they are derived, but allows the ligand termini to move with respect to each other. The geometry thus obtained is analogous to the GCLC model upon relaxation of the pinning constraint (*i.e.* the blue traces of the Main Text, Figure 9).

It is potentially informative to visualise the atomic displacements incurred by the steric interaction in a manner analogous to that illustrated for the graphene nanosheets illustrated in the Main Text, Figure 14. This is illustrated here in Figure 3. These subfigures indicate the absolute Cartesian displacement of each non-hydrogen atom between the optimisations used to obtain  $E_1$  and  $E_2$ , by a least-squares fit achieved with the `align` function of PyMOL. It should be noted that whilst the core oxo-metal complexes of each model do move as a result of removing the steric influence of the graphene sheet, these core complexes move as an essentially rigid unit, recapitulating the data illustrated in the Main Text, Figure 12, and forming a virtually invariant core around which the `align` procedure has optimised the fit. This accounts for the homogeneity of the shading of these atoms. With this in mind, the most important features of these geometries are therefore those with the greatest atom-to-atom difference in distortion. Particularly, the amide nitrogen and oxygen atoms are substantially distorted by relaxation, indicating a distortion with respect to the amide

carboxylate carbon. As indicated elsewhere, these atomic displacements are readily explicable by the removal of a steric clash between the amide nitrogen proton and a salient proton of the graphene zig-zag edge. Modulation of the  $sp^2/sp^3$  character of the amide nitrogen by the steric interaction has secondary effects on the PMPAB/MMPAB ligand conformations, and by extension the relative position of the oxo-metal cluster with respect to the graphene edge. Nevertheless, the internal geometry of the cluster is largely unperturbed.

## References

- [1] J. Klein et al. "New Way for Probing Bond Strength". In: *The Journal of Physical Chemistry A* 124.9 (Feb. 2020), pp. 1850–1860. doi: 10.1021/acs.jpca.9b09845.